

# Mechanism for vorticity in a secondary flow within a pipe: Vortex-induced vortex

Cite as: Phys. Fluids **32**, 033602 (2020); <https://doi.org/10.1063/1.5128414>

Submitted: 19 September 2019 . Accepted: 06 February 2020 . Published Online: 02 March 2020

L. M. Lin , and Y. X. Wu

## COLLECTIONS

Paper published as part of the special topic on [Advances in Micro/Nano Fluid Flows: In Memory of Prof. Jason Reese and Collection](#)



View Online



Export Citation



CrossMark

## ARTICLES YOU MAY BE INTERESTED IN

[On the influence of two-dimensional hump roughness on laminar-turbulent transition](#)

Physics of Fluids **32**, 034102 (2020); <https://doi.org/10.1063/1.5131577>

[Surface wave mechanism for directional motion of droplet on an obliquely vibrated substrate](#)

Physics of Fluids **32**, 031701 (2020); <https://doi.org/10.1063/1.5143874>


[Identifying improved microchannel configuration with triangular cavities and different rib structures through evaluation of thermal performance and entropy generation number](#)

Physics of Fluids **32**, 033601 (2020); <https://doi.org/10.1063/1.5137842>



CHALLENGE THE IMPOSSIBLE  
WITH OUR PRACTICAL REFERENCE GUIDES

Learn more 



# Mechanism for vorticity in a secondary flow within a pipe: Vortex-induced vortex

Cite as: Phys. Fluids 32, 033602 (2020); doi: 10.1063/1.5128414

Submitted: 19 September 2019 • Accepted: 6 February 2020 •

Published Online: 2 March 2020



View Online



Export Citation



CrossMark

L. M. Lin<sup>1,a)</sup>  and Y. X. Wu<sup>1,2</sup>

## AFFILIATIONS

<sup>1</sup>Key Laboratory for Mechanics in Fluid Solid Coupling Systems, Institute of Mechanics, Chinese Academy of Sciences, Beijing 100190, China

<sup>2</sup>School of Engineering Sciences, University of Chinese Academy of Sciences, Beijing 100049, China

<sup>a)</sup>Author to whom correspondence should be addressed: [llmbirthday@163.com](mailto:llmbirthday@163.com)

## ABSTRACT

Vortex-induced vortex theory, commonly used for a flow past a disturbed bluff body, is applied in this paper to analyze an incompressible flow through a circular-section pipe with the occurrence of a secondary flow. The disturbed flow field is solved based on the Stokes equations by introducing a vortex or vortex pair uniformly distributed along the axial direction and periodically varying along the azimuthal direction as a result of the secondary flow with the assumption of inertial force being neglected and the viscous force being dominant in the vicinity of the pipe walls. Two kinds of boundary cases are considered to simulate the introduced vorticity distributed on and near the walls, and two sign laws for vorticity are also derived and verified for the present internal flow. For original pipe flow with a specific velocity distribution, such as a paraboloid of revolution at lower Reynolds numbers, these two sign laws are all positive upstream but negative downstream and they physically reveal the intrinsic relationships of the vorticity sign among different vorticity components, which are generated inherently with specific signs in secondary flows. Furthermore, two basic viscous force mechanisms are identified: a direct effect for vorticity generated on the walls due to shear flows and an indirect effect for vorticity induced by a vortex with former vorticity near the walls. Examples to demonstrate these two sign laws under geometric disturbances at a laminar Reynolds number of 200 and physical meaning are also presented briefly.

Published under license by AIP Publishing. <https://doi.org/10.1063/1.5128414>

## I. INTRODUCTION

As a basic internal flow, pipe flow is employed in a wide range of engineering applications, such as marine pipelines used to convey single or multiphase fluid media (oil, gas, and water) and, more recently, separation of oil and water carried through specially designed pipes. Similarly, pipe flow could also be regarded as flow through an open channel or a duct and wind tunnel for hydrodynamic and aerodynamic experiments. The typical cross section of a pipe is circular; nevertheless, such an internal flow is commonly complicated due to not only geometric disturbances, but also turbulence. It is closely related to the physical mechanism responsible for the formation of vorticity along the walls, which is an important consideration in vortex dynamics.

For a circular-section pipe, the axial flow is commonly dominant. In a laminar state, the velocity profile is parabolic, that is, the axial velocity nonlinearly decreases from the maximum at the

center to zero at the wall. Within a turbulent flow at a high influx rate, the mean axial velocity first increases rapidly in the boundary layer and then increases slowly out of the boundary layer. However, regardless of whether the flow is laminar or turbulent, only azimuthal (time-averaged) vorticity is predominantly generated on the pipe wall.

Except for such a primary axial flow, subordinate secondary flows are generated under several circumstances. The first is the introduction of large-scale geometric disturbances into a common pipe, i.e., with a circular cross section and straight centerline. The characteristic length is mostly equivalent to the pipe diameter. Such disturbances can be represented by non-circular cross sections (e.g., rectangular, triangular, or trapezoidal), radial variations in the diameter, or axially curved pipes, all of which are reviewed in the literature.<sup>1</sup> For example, secondary flows could exist in a straight pipe with a non-circular cross section; as a result, the velocities at the corners will be very large. These secondary flows are

characterized by a fluid that flows toward the corner along the bisectrix of the angle and then outward in both directions. Such secondary flows continuously transport momentum from the center to the corners and generate high velocities there. These secondary flows also play important roles in open channels or square ducts,<sup>2</sup> as they lead to a reduction in the effective region in the measured experimental data. Through numerical simulations, close connection between Reynolds stress on the horizontal wall close to the corner and the interaction of bursting events between the horizontal and inclined walls is found in hexagonal ducts.<sup>3</sup> This interaction leads to the formation of the secondary flow. Even when the radius of the corner is rounded to minimize the inhomogeneous interactions associated with near-wall events, a cross-flow still appears that is similar to that found in ducts with sharp corners.<sup>4</sup> Recently, the secondary flow of Prandtl's second kind was simulated in fully developed spanwise-periodic channels with in-plane sinusoidal walls by direct numerical simulations,<sup>5</sup> which included the multiscale nature of the secondary flow. In such wavy channels, two counter-rotating streamwise vortices are present for each wavelength such that the secondary flow is directed from the corner of the channel to the wall along the centerplanes of the valleys; then, the flow turns in the wall-tangent direction along the wall and leaves the near-wall region through the peaks.

The second set of circumstances is the introduction of small-scale disturbances, such as a three-dimensional (3D) intrinsic instability (e.g., a T-S wave or horse-shoe and hairpin vortices in the boundary layer of a flat plate) in the transition region, local turbulent flow due to small-scale eddies, surface roughness and obstacles (e.g., a rock or a clod of mud stuck to the wall), and notches for circular pipes. For instance, simulations of the two-dimensional (2D) and 3D roughness by the superposition of sinusoidal surfaces with varying roughness heights and wavelengths revealed that streaky structures persist near the wall and are selectively modified by the roughness.<sup>6</sup> While these structures are abruptly broken by 2D roughness elements, as the infinite spanwise length of a roughness element allows for the fluid to flow only over and not around the roughness element, the arrangements of such roughness elements can substantially alter turbulent near-wall flow; such arrangements include cube array roughness elements in a staggered arrangement,<sup>7</sup> rectangular prism-shaped roughness elements<sup>8</sup> and converging-diverging riblets.<sup>9</sup> In recent years, scholars have discovered that the spanwise heterogeneity of roughness elements causes secondary flows that disrupt the near-wall cycle at the boundary with a critical parameter, namely, the ratio of the spanwise length scale of the roughness heterogeneity to the boundary layer thickness.<sup>10</sup> Accordingly, the outer layer similarity, as well as the occurrence of secondary flows, depends on the ratio of the roughness spanwise spacing to the boundary layer thickness.<sup>11</sup>

The third set of circumstances is a change in the incoming flow not only along the axial direction but also along the other directions, mainly the wall-tangent direction, caused by adopting a specific mechanism, such as a swirling flow through the azimuthal inlet of a cylindrical cyclone<sup>12,13</sup> or a guide vane installed in the center of a pipe.<sup>14–16</sup> In such a rotational flow, the length scale is rather large and approximates the pipe diameter.

In summary, these secondary flows not only result in the generation of axial vorticity on and near pipe walls, but also play an important role in organizing a complex pipe flow associated with

the motion and evolution of vorticity and vortices as well as with the interactions between vortices and pipe walls; hence, secondary flows constitute an important component of the vorticity and vortex dynamics in an internal flow. However, few studies have investigated the radial vorticity component, including its spatial distribution and physical relationships with other vorticity components in the above mentioned secondary flows; the same is true for the sign laws identified in the wake of a bluff body, which will be discussed as follows.

Recently, an interesting physical phenomenon was discovered in a flow passing by peak-perforated conic shrouds at a Reynolds number of 100.<sup>17</sup> As shown in Fig. 1, the strong effect of a conic disturbance with a wavy steepness  $W/\lambda$ , where  $W$  and  $\lambda$  are the non-dimensional wave height and wavelength, respectively, of the introduced conic disturbance, is taken as a typical example. The dominant vorticity is characterized by a special distribution with a specific sign in the near-wake region. For example, at a certain spanwise position of  $z = \frac{1}{4}\lambda$ , as shown in Fig. 1, the streamwise vorticity  $\omega_x$  with opposite signs is distributed alternatively in the upper and lower shear layers, but the vertical vorticity  $\omega_y$  is quite large with a single sign. Generally, the spanwise vorticity  $\omega_z$  is mainly negative in the upper shear layer, but positive in the lower shear layer. For convenience, in this phenomenon, the three vorticity components with specific signs can be described by  $(+|\omega_x|, +|\omega_y|, \text{ and } -|\omega_z|)$  in the upper shear layer and  $(-|\omega_x|, +|\omega_y|, \text{ and } +|\omega_z|)$  in the lower shear layer at  $z = \frac{1}{4}\lambda$ , whereas they can be described by  $(-|\omega_x|, -|\omega_y|, \text{ and } -|\omega_z|)$  in the upper shear layer and  $(+|\omega_x|, -|\omega_y|, \text{ and } +|\omega_z|)$  in the lower shear layer at  $z = \frac{3}{4}\lambda$ .

Based on the above four groups of sign combinations for the three vorticity components in shear layers, two sign laws are first summarized<sup>18</sup> and then theoretically confirmed by vortex-induced vortex (VIVor) theory,<sup>19</sup> as shown in Fig. 1. For the first sign law across the span, the sign of  $\omega_x \cdot \omega_y$  is always positive in the top shear layer but negative in the bottom shear layer. For the second sign law, the sign of  $\omega_x \cdot \omega_y \cdot \omega_z$  is always negative in both the top and bottom shear layers. These sign laws reveal the intrinsic relationship among the three vorticity components and help us further understand wake vortex dynamics.

In light of previous studies on secondary flows and the present sign laws in the wake of a bluff body, a curious question naturally arises, that is, whether similar sign laws appear in an internal flow through a pipe, particularly, when the secondary flows mentioned above are generated. The main aim of the present paper is to apply VIVor theory for an incompressible flow through a straight pipe as a basic internal flow to obtain the vorticity sign characteristics and to determine the basic physical mechanism responsible for generating these complex secondary flows. The problem how vorticity might be generated either on a wall or near to a wall, associated with the above secondary flows, is not discussed here. In Sec. II, the VIVor theory for pipe flow is briefly introduced. Two types of boundary cases are taken into account for different circumstances of vortex evolution. In Sec. III, three sign laws, namely, for radial and axial vorticity components only, for all three vorticity components, and for radial and axial velocity components, are presented under their unique conditions. Examples are illustrated at a laminar Reynolds number of 200. However, the physical meaning is discussed. Finally, the conclusions are presented in Sec. IV.

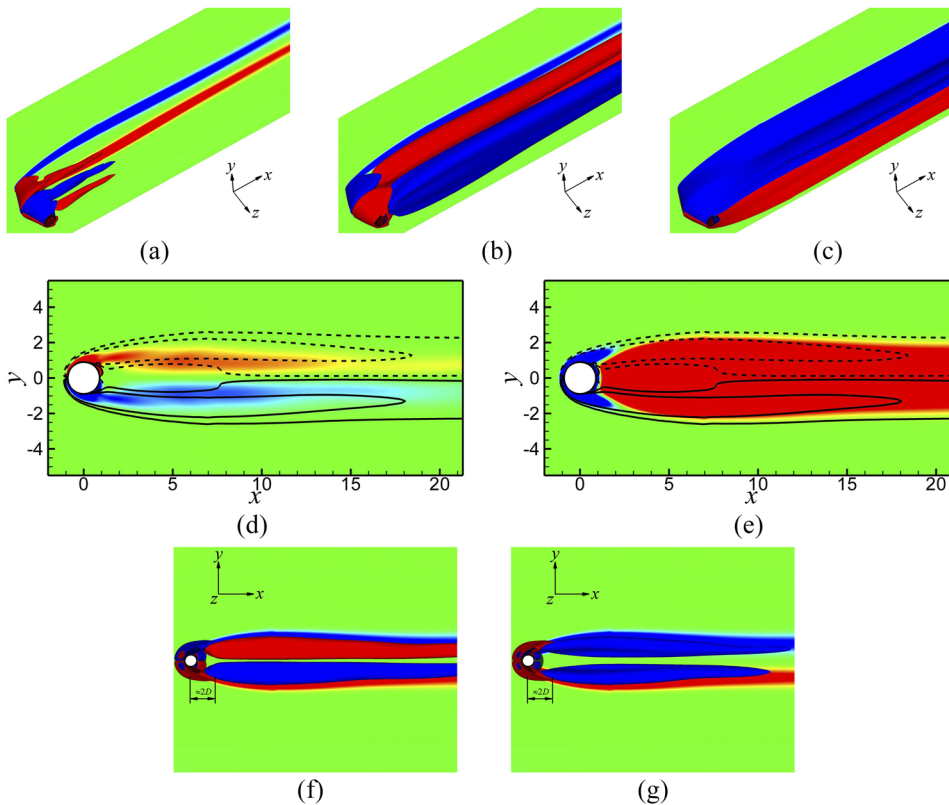


**FIG. 1.** Iso-surfaces of (a)  $\omega_x = \pm 0.2$ , (b)  $\omega_y = \pm 0.2$ , and (c)  $\omega_z = \pm 0.2$  [Reproduced with permission from L. M. Lin, X. F. Zhong, and Y. X. Wu, "Effect of perforation on flow past a conic cylinder at  $Re = 100$ : Vortex-shedding pattern and force history," *Acta Mech. Sin.* **34**, 238–256 (2018). Copyright 2017 Springer Nature], color contours of (d)  $\omega_x$  and (e)  $\omega_y$  at  $z = \frac{1}{4}\lambda = 1$ , and iso-surfaces of (f)  $\omega_x \cdot \omega_y = \pm 0.01$  and (g)  $\omega_x \cdot \omega_y \cdot \omega_z = \pm 0.01$  [Reproduced with permission from Lin *et al.*, "Mechanism of wavy vortex and sign laws in flow past a bluff body: Vortex-induced vortex," *Acta Mech. Sin.* **35**, 1–14 (2019). Copyright 2018 Springer Nature.] in a flow passing through a circular-section cylinder with a conic disturbance at  $t = 230$ ,  $\lambda = 4$ ,  $W/\lambda = 0.2$ , and  $Re = 100$ , where the red and blue colors as well as the solid and dashed contours of  $\omega_z = \pm 0.1$  and  $\pm 0.5$  in (d) and (e) denote the positive and negative values, respectively. In the sub-figures showing the iso-surfaces, the contours of  $\omega_z$  at  $z = 0$  are presented as the background.

**II. VORTEX-INDUCED VORTEX (VIVor) THEORY**

As reported in a previous study,<sup>19</sup> the VIVor theory is intended to illustrate the resultant vorticity and velocity fields induced by introducing a specific vortex (or vortex pair) under a particular set of boundary conditions. In the present circumstance of the typical internal flow through a pipe with a circular cross section shown in Fig. 2, the characteristics of the 3D vorticity field are theoretically investigated.

**A. Basic assumptions and preconditions in the flow analysis**

Before presenting the governing equations for the internal flow considered herein, some basic assumptions and preconditions are listed as follows:

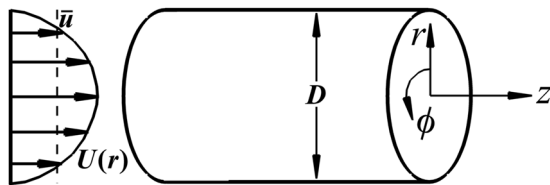


**FIG. 2.** Sketch of a flow through a circular-section pipe in a cylindrical coordinate system.

- (A1) A local cylindrical coordinate system  $(r, \phi, z)$  is established, in which  $r, \phi,$  and  $z$  denote the radial, azimuthal, and axial coordinates, respectively, as shown in Fig. 2. Moreover, the local pipe flow in this local system is consistent with the pipe flow at the inlet, i.e., the  $+z$ -axis is aligned with  $+|U(r)|$ , except for some recirculation regions or reversed flows where the local pipe flow is opposite to the incoming flow, i.e.,  $-|U(r)|$ , a typical example of which is a local flow separated from the wall.
- (A2) The incoming stream is a typical pipe flow with only an axial velocity  $U(r)$  and a cross-sectional averaged velocity  $\bar{u}$ , indicating that there merely exists an initial tangential vorticity  $\Omega_\phi(r)$  that always has a positive sign on the walls.
- (A3) The density  $\rho$  and viscosity  $\mu$  of the fluid as well as the kinematic viscosity,  $\nu = \mu/\rho$ , are constants, and, thus, the flow is incompressible.
- (A4) The pipe is straight without any geometric disturbances along the  $z$ -axis or in the  $(r, \phi)$  plane.
- (A5) The body forces, e.g., the gravitational force, are conservative.
- (A6) The transport of energy is ignored without any change in temperature.
- (A7) The introduced axial vortex or vortex pair with an axial vorticity  $\omega_z$ , which occurs naturally as a result of secondary flows near the pipe wall is first assumed to be distributed uniformly and locally along the  $z$ -axis, i.e., along the finite

axial length  $\lambda_z$  or  $z \in (0, \pm\lambda_z)$ . Conveniently, a pair of vortices with opposite signs is varied periodically along the circumferential direction with a non-dimensional wavelength of  $\lambda$ , as shown in Fig. 3. Furthermore, at the start of  $z = 0$  and  $r < R$  (where  $R$  is the pipe radius), there is only an introduced axial vorticity, and the radial and azimuthal vorticity components, namely,  $\omega_r$  and  $\omega_\phi$ , respectively, are zero.

(A8) The flow in the immediate neighborhood of the pipe walls at a normal distance  $h$ , i.e.,  $r \in [R - h, R]$ , is analyzed, similar to the work of Lin *et al.*<sup>19</sup> In such a region, viscous forces are dominant and inertial forces can be neglected. Based on an analysis of Kelvin’s circulation theorem,<sup>20</sup> the circulation and vorticity flux are always invariant if only a single vortex with a specific sign is taken into account. This condition indicates that the evolution of the sign of the vorticity is also unchanged and unaffected only by the inertial forces. It is well known that inertial forces play an important role in the evolution of nonzero vorticity, such as convective and stretching effects.<sup>21</sup> However, inertial forces are not intrinsically fundamental for the generation of vorticity, which is, instead, determined by viscous forces under the present circumstances. In this sense, the following can be anticipated: at a certain low Reynolds number, a near-wall vorticity would be dissipated quickly far away from the walls due to relatively high viscous forces, even though this vorticity is induced by a certain disturbance (similar to a 3D instability); in contrast, at a sufficiently high Reynolds number, such an induced vorticity would be transported outside and downstream and possibly shed from the walls owing to the relatively strong effect of inertial forces. Therefore, the present flow analysis can be carried out without inertial forces in the local nearest-wall region to investigate the evolution of the sign of the vorticity. On the other hand, such a local region is also occupied mainly by an axial vorticity with a specific sign, while an opposite-signed axial vorticity appears in the outer layer far away from the wall.<sup>11</sup> Therefore, in consideration of the (A7) above, we simply take such axial vorticity on and near the wall into account in the following analysis.

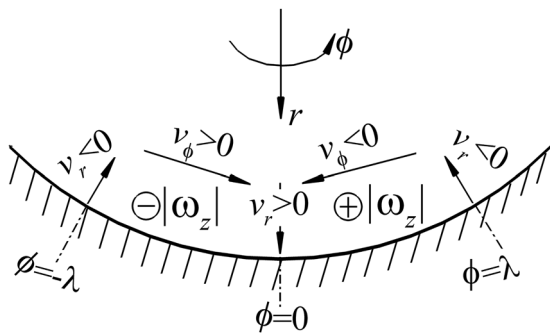


**FIG. 3.** Sketch of the introduced axial vortex pair ( $-|\omega_z|$ ,  $+|\omega_z|$ ) distributed on or near the walls of a circular-section pipe and periodically along the circumferential direction  $\phi$  in a certain sectional plane  $(r, \phi)$ , where the symbols  $\oplus$  and  $\ominus$  denote positive and negative signs of  $\omega_z$ , respectively.

### B. Governing equations in an internal flow

Based on the above conditions, the governing equations, i.e., the mass conservation and momentum equations, are written in non-dimensional forms as follows:

$$0 = \frac{\partial v_r}{\partial r} + \frac{v_r}{r} + \frac{1}{r} \frac{\partial v_\phi}{\partial \phi} + \frac{\partial v_z}{\partial z}, \tag{1a}$$

$$\frac{\partial p}{\partial r} = \frac{1}{Re} \left( \frac{\partial^2 v_r}{\partial r^2} + \frac{1}{r} \frac{\partial v_r}{\partial r} - \frac{v_r}{r^2} + \frac{1}{r^2} \frac{\partial^2 v_r}{\partial \phi^2} - \frac{2}{r^2} \frac{\partial v_\phi}{\partial \phi} + \frac{\partial^2 v_r}{\partial z^2} \right), \tag{1b}$$

$$\frac{1}{r} \frac{\partial p}{\partial \phi} = \frac{1}{Re} \left( \frac{\partial^2 v_\phi}{\partial r^2} + \frac{1}{r} \frac{\partial v_\phi}{\partial r} - \frac{v_\phi}{r^2} + \frac{1}{r^2} \frac{\partial^2 v_\phi}{\partial \phi^2} + \frac{2}{r^2} \frac{\partial v_r}{\partial \phi} + \frac{\partial^2 v_\phi}{\partial z^2} \right), \tag{1c}$$

$$\frac{\partial p}{\partial z} = \frac{1}{Re} \left( \frac{\partial^2 v_z}{\partial r^2} + \frac{1}{r} \frac{\partial v_z}{\partial r} + \frac{1}{r^2} \frac{\partial^2 v_z}{\partial \phi^2} + \frac{\partial^2 v_z}{\partial z^2} \right), \tag{1d}$$

where  $v_r$ ,  $v_\phi$ , and  $v_z$  denote the velocity components in their corresponding cylindrical coordinate directions,  $p$  is the static pressure still scaled by  $\rho \bar{u}^2$ , and  $Re$  is the Reynolds number based on the mean velocity in a pipe  $\bar{u}$  and the characteristic diameter of the pipe  $D$ , i.e.,  $Re = \bar{u}D/\nu$ . The velocities are scaled by  $\bar{u}$  and the lengths by  $D$ . These equations must be supplemented with the proper boundary conditions, namely, those expressing the absence of slip in the fluid at the pipe walls  $r = R$ :  $v_r = v_\phi = v_z = 0$ , where  $R$  is the non-dimensional radius of the pipe actually equal to 0.5. Correspondingly, the solutions prevail in the range from  $R - h$  to  $R$ , i.e.,  $r \in [R - h, R]$  and  $z \in (0, \pm\lambda_z)$ .

### C. Theoretical solutions of vortex-induced velocity and vorticity fields

Because non-linear inertial forces are ignored according to assumption (A8), the principle of superposition of different velocity fields can, thus, be applied in the further analysis of Eq. (1). Accordingly, the local flow field in the pipe can be divided into two parts. The first part is the 2D or axisymmetric original flow (relative to the following induced flow) with velocity  $U(r)$  through the pipe without any 3D perturbation. The second part is the resultant 3D flow field with an induced velocity  $(v_r, v_\phi, v_z)$  and vorticity  $(\omega_r, \omega_\phi, \omega_z)$ , mainly in secondary flows caused by a 3D geometric disturbance, e.g., a non-circular cross section, and in the transition region from a laminar regime to a turbulent regime after the critical Reynolds number is reached, as mentioned before. VIVor theory is initially focused on the induced flow fields,  $(v_r, v_\phi, v_z)$  and  $(\omega_r, \omega_\phi, \omega_z)$ , without the original flow; then, the coupled effects of these two flow field parts,  $(v_r, v_\phi, U + v_z)$  and  $(\omega_r, \Omega_\phi + \omega_\phi, \omega_z)$ , are considered.

Here, two concepts regarding induction in a VIVor and an induced velocity/vorticity field are clearly explained. First, induction in a VIVor indicates that the vortex is induced by the introduced vortex, which already exists or is generated early. Second, the velocity and vorticity fields with all three components are induced by any kind of 3D disturbance, such as a geometric disturbance. Therefore, the second kind of induction distinguishes

the different physical mechanisms responsible for generating vorticity, while the first kind simply illustrates the physical relationship among the different components of vorticity already generated.

Two kinds of boundary cases are applied in flow analysis. The first type of boundary is the introduced vorticity generated on the walls, corresponding to the disturbed vortices attached to the present positions. The second boundary is the introduced vorticity distributed near the walls and reduced to zero on the walls; this vorticity is related to the already or earlier generated vortices convected or evolved downstream. In addition, if the vortex moves into the outer layer ( $r < R - h$ ) and then induces the vorticity with an opposite sign on the walls, it could be treated similar to the first situation but with opposite signs.

As shown in Fig. 3, on the basis of assumption (A7), an introduced axial vortex pair centered around  $z = 0$  with opposite signs is distributed uniformly along the  $z$ -axis on or near the inner side of the straight circular-section pipe. Such induced vorticity varies periodically along the azimuthal direction with the non-dimensional azimuthal wavelength  $\lambda$  and gradually disappears far away from the inner walls ( $r \rightarrow 0$ ).

The induced velocities, mainly for the radial and azimuthal components, which are associated with the introduced axial vortex according to the Biot–Savart law and are, therefore, independent of  $z$  according to assumption (A7), are assumed as

$$v_r(r, \phi) = A_r(r) \cos(k\phi), \tag{2a}$$

$$v_\phi(r, \phi) = -A_\phi(r) \sin(k\phi), \tag{2b}$$

where  $A_r$  and  $A_\phi$  are the positive and dimensionless amplitudes of  $v_r$  and  $v_\phi$ , respectively, and  $k$  is the non-dimensional wave number,  $k = \pi/\lambda$ . Here, the maximal wavelength is  $2\pi R$  and scaled by  $D$ ; therefore,  $\lambda \leq \pi$  and  $k \geq 1$ . Because the azimuthal periodicity for a circular pipe represents a single cycle from head to tail, different from the spanwise periodicity for a bluff body with an infinite span,  $k$  also indicates the number of introduced disturbed vortex pairs and is, therefore, a natural number,  $k \in N$ .

Consequently, by substituting the above radial and azimuthal components of the induced velocity shown in Eq. (2) in the continuity equation, Eq. (1a), the axial component is obtained as

$$v_z(r, \phi, z) = -z \left( \frac{dA_r}{dr} + \frac{A_r}{r} - k \frac{A_\phi}{r} \right) \cos(k\phi) + C_z(r, \phi), \tag{3}$$

where  $C_z(r, \phi)$  is an unknown coefficient.

Therefore, the three components of the induced vorticity are defined in the cylindrical coordinate system as follows:

$$\begin{aligned} \omega_r &= \frac{1}{r} \frac{\partial v_z}{\partial \phi} - \frac{\partial v_\phi}{\partial z} \\ &= \frac{kz}{r} \left( \frac{dA_r}{dr} + \frac{A_r}{r} - k \frac{A_\phi}{r} \right) \sin(k\phi) + \frac{1}{r} \frac{\partial C_z}{\partial \phi}, \end{aligned} \tag{4a}$$

$$\begin{aligned} \omega_\phi &= \frac{\partial v_r}{\partial z} - \frac{\partial v_z}{\partial r} \\ &= z \frac{d}{dr} \left( \frac{dA_r}{dr} + \frac{A_r}{r} - k \frac{A_\phi}{r} \right) \cos(k\phi) - \frac{\partial C_z}{\partial r}, \end{aligned} \tag{4b}$$

$$\begin{aligned} \omega_z &= \frac{\partial v_\phi}{\partial r} + \frac{v_\phi}{r} - \frac{1}{r} \frac{\partial v_r}{\partial \phi} \\ &= - \left( \frac{dA_\phi}{dr} + \frac{A_\phi}{r} - k \frac{A_r}{r} \right) \sin(k\phi). \end{aligned} \tag{4c}$$

Correspondingly, under the non-slip boundary conditions and the present vorticity distribution limited only to the local flow region in assumption (A7), that is,  $r \in [R - h, R]$  and  $z \in (0, \pm\lambda_z)$  according to (A7) we have

$$C_z(r, \phi) = 0, \tag{5a}$$

$$A_r|_{r=R} = 0, \tag{5b}$$

$$A_\phi|_{r=R} = 0, \tag{5c}$$

$$\left. \frac{dA_r}{dr} \right|_{r=R} = 0. \tag{5d}$$

In flow analysis, it is convenient to eliminate the pressure  $p$  in the momentum equations, Eqs. (1b)–(1d). On the other hand, through observing the vorticity components in Eq. (4), the following two functions can be defined:

$$X(r) = \frac{dA_r}{dr} + \frac{A_r}{r} - k \frac{A_\phi}{r}, \tag{6a}$$

$$Y(r) = \frac{dA_\phi}{dr} + \frac{A_\phi}{r} - k \frac{A_r}{r}. \tag{6b}$$

Due to the special distributions of the velocity and vorticity fields in the present study, we consider two relationships. The first relationship states that Eqs. (1b) and (1c) are independent of the axial coordinate  $z$ . Therefore, one unsolved function about  $X(r)$  is obtained based on Eq. (1d) as follows:

$$\frac{\partial^2 p}{\partial \phi \partial z} = 0, \quad \Rightarrow \quad \frac{d^2 X}{dr^2} + \frac{1}{r} \frac{dX}{dr} - \frac{k^2}{r^2} X = 0. \tag{7}$$

The second relationship describes the cross-partial derivative between Eqs. (1b) and (1c). As a result, another unsolved function about  $Y(r)$  is obtained as follows:

$$\frac{d^2 Y}{dr^2} + \frac{1}{r} \frac{dY}{dr} - \frac{k^2}{r^2} Y = 0. \tag{8}$$

### 1. The first boundary case (f.b.c.): Vorticity generated on the walls

In the f.b.c., the axial vorticity is generated with a constant amplitude of intensity  $A_{\omega_z} (>0)$ , which is assumed to be maximal on the wall. Thus, with the aid of Eqs. (5b), (5c), and (4c) and in consideration of the present flow in the cylindrical coordinate system, we have

$$|\omega_z|_{r=R} = A_{\omega_z}, \quad \Rightarrow \quad - \left. \frac{dA_\phi}{dr} \right|_{r=R} = A_{\omega_z} > 0. \tag{9}$$

Introducing the transformation  $\gamma = \ln r$ , Eqs. (7) and (8) can be rewritten as

$$\frac{d^2 X}{d\gamma^2} - k^2 X = 0, \quad \text{with} \quad X|_{r=R} = 0, \tag{10a}$$

$$\frac{d^2 Y}{d\gamma^2} - k^2 Y = 0, \quad \text{with} \quad Y|_{r=R} = -A_{\omega_z}. \tag{10b}$$

As a result, taking into account the boundary condition in Eq. (4c), describing the intensity of the axial vorticity on the pipe walls, the solutions of Eq. (10) can be obtained as follows:

$$X(r) = \frac{dA_r}{dr} + \frac{A_r}{r} - k \frac{A_\phi}{r} = C_1 (r^k - R^{2k} r^{-k}), \tag{11a}$$

$$Y(r) = \frac{dA_\phi}{dr} + \frac{A_\phi}{r} - k \frac{A_r}{r} = -C_2 r^k, \tag{11b}$$

where  $C_1$  and  $C_2$  are both positive constants. Equation (10b) gives  $C_2 = A_{\omega_z} R^{-k}$ .

Furthermore, by eliminating  $A_r$ , Eq. (11) gives the following relationship:

$$\frac{d^2 A_\phi}{dr^2} + \frac{3}{r} \frac{dA_\phi}{dr} + \frac{1-k^2}{r^2} A_\phi = C_1 k (r^{k-1} - R^{2k} r^{-k-1}) - C_2 (k+2) r^{k-1}. \tag{12}$$

Thus, the above equation presents two sets of solutions: one with  $k = 1$  and another with  $k \geq 2$ .

**A: Special solutions with  $k = 1$**

Under the condition, where the wave number  $k = 1$ , Eq. (12) is simplified as

$$\frac{d^2 A_\phi}{dr^2} + \frac{3}{r} \frac{dA_\phi}{dr} = C_1 \left(1 - \frac{R^2}{r^2}\right) - 3C_2, \tag{13}$$

where  $C_2 = A_{\omega_z}/R$ . Introducing the transformation  $\Gamma = \frac{1}{r} \frac{dA_\phi}{dr}$  into Eq. (13), we have

$$r \frac{d\Gamma}{dr} + 4\Gamma = (C_1 - 3C_2) - C_1 \frac{R^2}{r^2}, \tag{14}$$

with condition  $\Gamma|_{r=R} = -C_2$ . The solution is obtained as follows:

$$\Gamma = \frac{C_1 - 3C_2}{4} - \frac{C_1}{2} \beta^{-2} + \frac{C_1 - C_2}{4} \beta^{-4}, \tag{15}$$

where  $\beta = r/R$  is the relative radial position. Then, with the boundary condition of Eq. (5), we have

$$A_r(\beta) = \frac{C_1}{8} R^2 (3\beta^2 + \beta^{-2} - 4) - \frac{C_1}{2} R^2 \ln \beta + \frac{C_2}{8} R^2 (2 - \beta^2 - \beta^{-2}), \tag{16a}$$

$$A_\phi(\beta) = \frac{C_1}{8} R^2 (\beta^2 - \beta^{-2}) - \frac{C_1}{2} R^2 \ln \beta + \frac{C_2}{8} R^2 (2 - 3\beta^2 + \beta^{-2}), \tag{16b}$$

with the following conditions:

$$C_1 \in \left[ \frac{3}{2} C_2, 3C_2 \right), C_2 = \frac{A_{\omega_z}}{R}, h = (1 - \beta_0)R, \tag{17}$$

$$\beta_0 = \sqrt{\frac{\sqrt{4C_1 C_2 - 3C_2^2} - C_1}{3C_2 - C_1}}.$$

The variations in the amplitudes of the radial and azimuthal velocity components,  $A_r$  and  $A_\phi$ , respectively, with the relative radial position  $\beta$  are shown in Fig. 4 with  $C_1 = 2C_2$ . Evidently,  $A_\phi$  almost linearly increases toward the center of the pipe, while  $A_r$  gradually increases away from the pipe wall. In association with the axial vorticity introduced on the pipe wall and the non-slip boundary conditions, Fig. 4 shows that the magnitude of  $A_\phi$  is greater than that of  $A_r$ , and thus,  $v_\phi$  is larger than  $v_r$ .

Correspondingly, the induced axial velocity  $v_z$  is also obtained as

$$v_z = C_1 z R (\beta^{-1} - \beta) \cos \phi. \tag{18}$$

The pressure  $p$  is presented as follows:

$$p = \frac{R}{Re} [(C_1 - C_2)\beta - C_1 \beta^{-1}] \cos \phi + C_p, \tag{19}$$

where  $C_p$  is a constant. Thus, the three vorticity components in Eq. (4) are given by

$$\omega_r = -C_1 z (\beta^{-2} - 1) \sin \phi, \tag{20a}$$

$$\omega_\phi = C_1 z (\beta^{-2} + 1) \cos \phi, \tag{20b}$$

$$\omega_z = C_2 R \beta \sin \phi. \tag{20c}$$

**B: Ordinary solutions with  $k \geq 2$**

Continually, introducing the transformation  $\gamma = \ln r$  in Eq. (12), we have

$$\frac{d^2 A_\phi}{d\gamma^2} + 2 \frac{dA_\phi}{d\gamma} - (k^2 - 1) A_\phi = [C_1 k - C_2 (k + 2)] e^{(k+1)\gamma} - C_1 k R^{2k} e^{-(k-1)\gamma}, \tag{21}$$

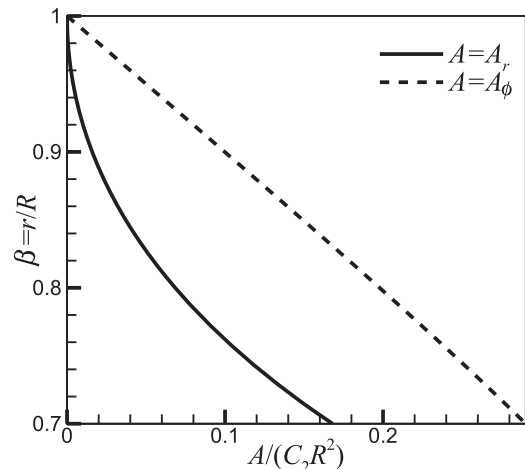


**FIG. 4.** Variations in the relative amplitudes,  $A_r$  and  $A_\phi$  in the nearest-wall region of the pipe divided by the product of  $C_2$  and  $R^2$ , in the f.b.c. with  $C_1 = 2C_2$  and  $k = 1$  with respect to the relative radial position  $\beta = r/R (\leq 1)$  away from the pipe walls.

with the boundary conditions of Eqs. (5c) and (9). Thus, considering Eq. (11b), we obtain the following solutions:

$$A_r(\beta) = \frac{C_1 R^{k+1}}{4} \left[ \frac{(k+2)\beta^{k+1} + k\beta^{-(k+1)}}{k+1} - \frac{k\beta^{k-1} + (k-2)\beta^{-(k-1)}}{k-1} \right] + \frac{C_2 R^{k+1}}{4} \left[ \beta^{k-1} - \frac{k\beta^{k+1} + \beta^{-(k+1)}}{k+1} \right], \quad (22a)$$

$$A_\phi(\beta) = \frac{C_1 k R^{k+1}}{4} \left[ \frac{\beta^{k+1} - \beta^{-(k+1)}}{k+1} - \frac{\beta^{k-1} - \beta^{-(k-1)}}{k-1} \right] - \frac{C_2 R^{k+1}}{4} \left[ (\beta^{k+1} - \beta^{k-1}) + \frac{\beta^{k+1} - \beta^{-(k+1)}}{k+1} \right], \quad (22b)$$

with the following requirements (at least):

$$C_1 > \frac{1}{2} C_2, \quad C_2 = A_{\omega_z} R^{-k}. \quad (23)$$

The variations in the amplitudes of the radial and azimuthal velocity components,  $A_r$  and  $A_\phi$ , respectively, with the relative radial position  $\beta$  and different wave numbers  $k \geq 2$  are shown in Fig. 5 with  $C_1 = C_2$ .  $A_r$  first increases slowly because  $dA_r/d\beta = 0$  at  $\beta = 1$  and then rapidly grows nonlinearly far away from the pipe wall; in contrast,  $A_\phi$  first increases almost linearly within a certain distance away from the inner wall of the pipe, but then quickly decreases beyond a certain distance. At the same radial position  $\beta$ , when the wave number  $k$  increases,  $A_r$  gradually increases, while  $A_\phi$  decreases. Moreover, where the present analysis is effective, the radial distance  $h$  away from the pipe wall becomes smaller with increasing wave number, as shown in Fig. 5(b). In fact, from the following physical explanation, we can also anticipate that as the wave number increases, the number of introduced disturbed vortex pairs also increases, indicating that the azimuthal region or wavelength for each vortex pair gradually decreases, as well as the radial region. As a result, the effective region of analysis decreases as well.

Hence, the induced axial velocity is obtained as

$$v_z = C_1 z R^k (\beta^{-k} - \beta^k) \cos(k\phi). \quad (24)$$

Meanwhile, the three components of the induced vorticity are expressed as

$$\omega_r = -C_1 z R^{k-1} k [\beta^{-(k+1)} - \beta^{k-1}] \sin(k\phi), \quad (25a)$$

$$\omega_\phi = C_1 z R^{k-1} k [\beta^{-(k+1)} + \beta^{k-1}] \cos(k\phi), \quad (25b)$$

$$\omega_z = C_2 R^k \beta^k \sin(k\phi). \quad (25c)$$

The above equations demonstrate that such solutions with  $k \geq 2$  include the special solutions at  $k = 1$  for only the induced vorticity and axial velocity, namely, Eqs. (20) and (18), respectively, although the derivation process is different.

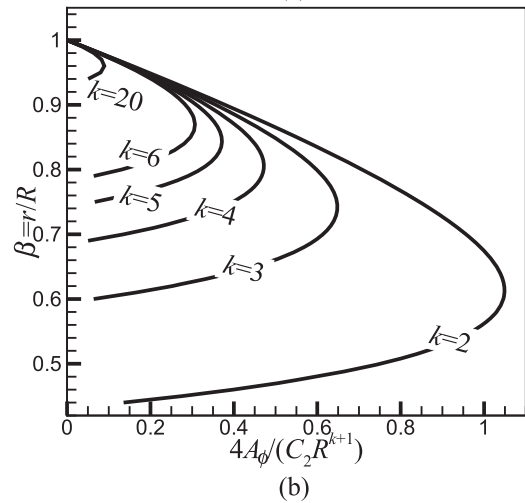
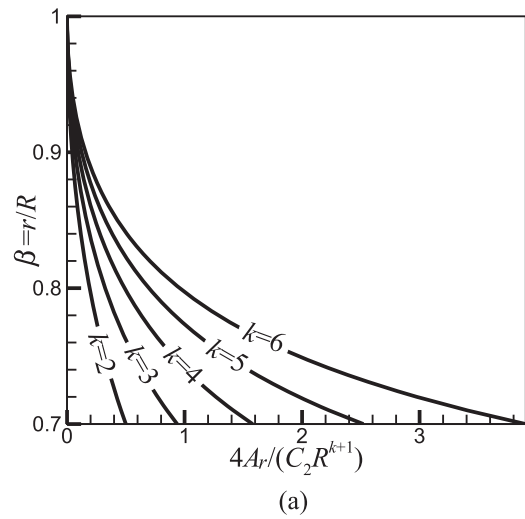


FIG. 5. Variations in the relative amplitudes (a)  $A_r$  and (b)  $A_\phi$  in the nearest-wall region of the pipe divided by  $\frac{1}{4} C_2 R^{k+1}$  in the f.b.c. with  $C_1 = C_2$  and different wave numbers  $k \geq 2$  with respect to the relative radial position  $\beta = r/R (\leq 1)$  away from the pipe walls. Notice that only amplitude values satisfying  $A_\phi \geq 0$  are presented in sub-figure (b).

### 2. The second boundary case (s.b.c.): Vorticity distributed near the walls

In the s.b.c., the axial vorticity is already generated upstream, after which it is convected into and distributed just above the present positions, and then it finally disappears on the pipe walls. Therefore, with the help of Eqs. (5b), (5c), and (4c), the disappearance of the axial vorticity on the pipe walls gives the following condition:

$$|\omega_z|_{r=R} = 0, \quad \Rightarrow \quad \left. \frac{dA_\phi}{dr} \right|_{r=R} = 0. \quad (26)$$

This condition is exactly the same as that for the radial amplitude  $A_r$  in Eq. (5d). Considering the governing equations of  $A_r$  and  $A_\phi$ , i.e., Eqs. (7) and (8), the same boundary conditions for  $A_r$  and  $A_\phi$ , as well



as those for  $X$  and  $Y$ , i.e.,  $X|_{r=R} = Y|_{r=R} = 0$ , would display the same variation along the radial position. The solutions in the inner region of the pipe walls,  $r \in [R - h, R]$ , are obtained as follows,

$$A_r = A_\phi = A, \tag{27a}$$

$$X = Y = \frac{dA}{dr} + \frac{1-k}{r}A = C(r^k - R^{2k}r^{-k}), \tag{27b}$$

where  $C$  is a positive constant. Similar to the f.b.c., two situations must be discussed individually: the special solutions with  $k = 1$  and the ordinary solutions with  $k \geq 2$ .

**A: Special solutions with  $k = 1$**

In the present condition where  $k = 1$  in Eq. (27b), we can obtain

$$A(\beta) = CR^2 \left( \frac{\beta^2 - 1}{2} - \ln \beta \right). \tag{28}$$

As shown in Fig. 6, the variations in the amplitudes of  $v_r$  and  $v_\phi$  in the present case are very similar to that of  $v_r$  in the f.b.c. shown in Figs. 4 and 5(a).

Therefore, the induced axial velocity is obtained as

$$v_z = CzR(\beta^{-1} - \beta) \cos \phi. \tag{29}$$

In addition, the pressure is given by

$$p = \frac{2CR\beta}{Re} \cos \phi + C_p, \tag{30}$$

where  $C_p$  is a constant. The three components of the vorticity are thus given by

$$\omega_r = -Cz(\beta^{-2} - 1) \sin \phi, \tag{31a}$$

$$\omega_\phi = Cz(\beta^{-2} + 1) \cos \phi, \tag{31b}$$

$$\omega_z = CR(\beta^{-1} - \beta) \sin \phi. \tag{31c}$$

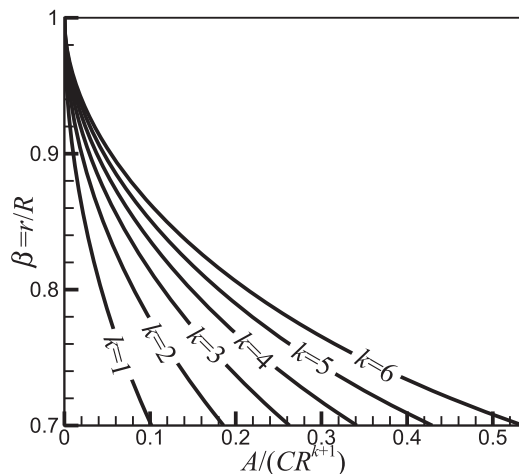


**FIG. 6.** Variations in the relative amplitude  $A$  in the nearest-wall region of the pipe divided by  $CR^{k+1}$  in the s.b.c. at different wave numbers  $k$  with respect to the relative radial position  $\beta = r/R (\leq 1)$  away from the pipe walls.

**B: Ordinary solutions with  $k \geq 2$**

In the present case, where  $k \geq 2$ , the solution of Eq. (27b) is obtained as

$$A(\beta) = \frac{CR^{k+1}}{2} \left[ \beta^{k+1} - \frac{k\beta^{k-1} - \beta^{-(k-1)}}{k-1} \right]. \tag{32}$$

As shown in Fig. 6 with  $k \geq 2$ , the variations in the amplitude  $A$  of  $v_r$  and  $v_\phi$  at different wave numbers along with the radial distance away from the pipe wall are also similar to either the same variations with  $k = 1$  or those of  $v_r$  in the f.b.c. in Fig. 5(a). Moreover, as the wave number increases, the amplitudes of both  $A_r$  and  $A_\phi$  gradually increase at a certain radial position.

Therefore, the induced axial velocity is obtained as

$$v_z = CzR^k(\beta^{-k} - \beta^k) \cos(k\phi). \tag{33}$$

Thus, the three components of the induced vorticity are thus given by

$$\omega_r = -CzR^{k-1}k[\beta^{-(k+1)} - \beta^{k-1}] \sin(k\phi), \tag{34a}$$

$$\omega_\phi = CzR^{k-1}k[\beta^{-(k+1)} + \beta^{k-1}] \cos(k\phi), \tag{34b}$$

$$\omega_z = CR^k(\beta^{-k} - \beta^k) \sin(k\phi). \tag{34c}$$

Similarly, the above equations show that such solutions include the solutions at  $k = 1$  mainly for the induced vorticity and axial velocity components, namely, Eqs. (31) and (29), respectively, although the derivation process is different.

**III. RESULTS**

**A. The first sign law for the radial and axial components of vorticity**

According to the above analysis of the spatial distributions of the radial and axial vorticity components in the f.b.c. and the s.b.c., the first sign law is obtained. As an example, Eqs. (25) and (34) for  $k \geq 2$  present the following relationship:

$$\omega_r \cdot \omega_z = \begin{cases} -C_1 C_2 z R^{2k-1} k \beta^{-1} (1 - \beta^{2k}) \sin^2(k\phi), & \text{in f.b.c.,} \\ -C^2 z R^{2k-1} k \beta^{-1} (\beta^{-k} - \beta^k)^2 \sin^2(k\phi), & \text{in s.b.c.,} \end{cases}$$

where  $r \in [R - h, R]$  in the inner region or the near-wall region of the pipe walls. Then, we can rewrite the above relationship by introducing the sign function,  $\text{sgn}(x)$ , and the first sign variable,  $\omega_1$ , as follows:

$$\text{sgn}(\omega_r \cdot \omega_z) = \text{sgn}(\omega_1) = \begin{cases} 1, & z < 0 \\ -1, & z > 0, \end{cases} \tag{35}$$

except for some specific positions (e.g.,  $\phi = 0$  and  $\lambda$ ) at which  $\omega_1 = 0$ , as well as that obtained from the solutions with  $k = 1$ . This relationship shows that  $\pm|\omega_z|$  induces  $\mp|\omega_r|$  in the downstream region ( $z > 0$ ) and  $\pm|\omega_z|$  induces  $\pm|\omega_r|$  in the upstream region

( $z < 0$ ). This relationship is referred to as the first sign law for the radial and axial components of the vorticity distributed within the internal flow through a pipe, as shown in Fig. 7, and clearly demonstrates that the first sign law for the secondary flow in a pipe is independent of the spatial distribution of both the induced azimuthal vorticity  $\omega_\phi$  and the original flow  $U(r)$ . The first sign law is also independent of the wave number  $k$  and Reynolds number  $Re$ . This indicates that the first sign law is an intrinsic physical mechanism for vorticity and vortex dynamics, regardless of the kind of disturbance resulting in the secondary flow.

On the other hand, the first sign law in the upstream region ( $z < 0$ ) is effective mainly when the introduced axial vortex or vortex pair always exists or is sustained. Considering this aspect, the disturbances leading to the generation of an induced axial vortex can be classified into two categories. The first category is an intermittent or random disturbance, such as the turbulence at large Reynolds numbers. The second category is a persistent disturbance, such as a geometric disturbance or surface roughness. For the stretching and convective mechanisms of non-linear inertial forces,<sup>21</sup> an axial vortex generated by the first category of disturbance is easily suppressed in the upstream region ( $z < 0$ ), but tends to evolve and convect into the downstream region ( $z > 0$ ) along with the original pipe flow  $+|U(r)|$ ; therefore, the first sign law is mostly dominant in the downstream region, where  $z > 0$ . For the second category of disturbance, similar to the analysis in the flow past the bluff body,<sup>19</sup> the first sign law is consistently effective in the upstream region, where  $z < 0$  and develops into the downstream region where  $z > 0$  in a certain range under the inertial effect of the local pipe flow  $+|U(r)|$ .

Interestingly, such a sign relationship between the radial and axial vorticity components is consistent with the first sign law for the streamwise and vertical components of the vorticity on the upper surface or upper side in the wake of a bluff body,<sup>19</sup> if we adopt condition  $R \rightarrow \infty$  and a local Cartesian coordinate system in the inner region of the pipe walls, where the vertical direction is perpendicular to the pipe walls and the streamwise direction is aligned along the pipe flow direction  $+|U(r)|$ . This suggests that the first sign law is universal in both an external flow past a bluff body and an internal flow in a pipe.

Moreover, the different effects of viscous forces are also distinguishable and can be classified into two types for both external and internal flows: a direct effect and an indirect effect. For

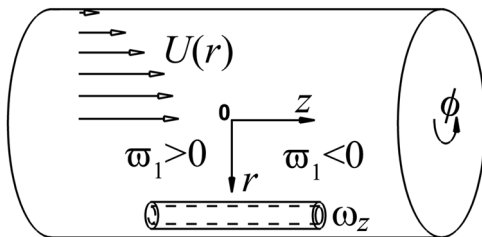


**FIG. 7.** Schematic of the first sign law for the radial and axial components of the vorticity distributed within the flow through a circular-section pipe caused by an introduced axial vortex or vortex pair uniformly distributed along the axial direction but periodically varying along the azimuthal direction, where  $U(r)$  (denoted by hollow arrows) is the velocity profile of the pipe flow.

example, in the present pipe flow, the introduced axial vortex with axial vorticity on the walls is the direct consequence of shear flow near the walls, i.e., secondary flows, which is also similar to the original tangential vorticity  $\Omega_\phi(r)$  due to the pipe velocity  $U(r)$ . However, the radial vorticity component is always zero on the pipe walls. Obviously, the appearance of radial vorticity is certainly not the result of the shear flow near the walls; rather, radial vorticity is induced by the present physical mechanism of the VIV or described by the Stokes equations that is dominated by viscous forces. Therefore, the direct effect of viscous forces leads to the generation of two wall-tangent vorticity components on the walls, while the generation of a single wall-normal vorticity component is the indirect effect of viscous forces.

### B. The second sign law for the three vorticity components

Before presenting the second sign law for the three components of the vorticity distributed within the flow through a pipe, let us review the basic laminar pipe flow solved with Hagen–Poiseuille theory at low Reynolds numbers.<sup>1</sup> Generally, the flow through a straight tube of circular cross section is the case with rotational symmetry corresponding to the case of 2D flow through a channel. As shown in Fig. 2, the original flow (relative to the nearest-wall flow induced by a disturbance) with axial velocity  $U(r)$  parallel to the axis of the pipe, that is, the  $z$ -axis, depends only on the radial coordinate. The velocity components in the radial and tangential directions are zero and the pressure is constant in every cross section. With the non-slip boundary condition on the pipe walls  $r = R$  or  $\beta = 1$ , the classic pipe flow solution gives the non-dimensional velocity distribution

$$U(r) = 2 \left( 1 - \frac{r^2}{R^2} \right) = 2(1 - \beta^2), \quad (36a)$$

$$\bar{u} = \frac{D^2}{32\mu} \left( -\frac{dP}{dZ} \right), \quad (36b)$$

where  $P$  is the dimensional pressure and  $Z$  is the dimensional axial coordinate. Such velocity over the cross section is distributed in the form of a paraboloid of revolution. Based on the definition of vorticity in Eq. (4), we have the following typical vorticity distribution:

$$\Omega_\phi = -\frac{dU(r)}{dr} = \frac{4r}{R^2} = \frac{4\beta}{R} \quad \text{and} \quad \Omega_r = \Omega_z = 0, \quad (37)$$

where  $\Omega_r$ ,  $\Omega_\phi$ , and  $\Omega_z$  are the radial, azimuthal, and axial vorticity components, respectively, due to the original pipe flow  $U(r)$ . This equation shows that the azimuthal vorticity is always positive, except at the pipe center with  $\Omega_\phi = 0$ , as shown in Fig. 8. Alternatively, this relationship can be expressed by

$$\text{sgn}(\Omega_\phi) = 1, \quad r \in (0, R]. \quad (38)$$

On the other hand, another assumption is introduced here. Compared with the magnitude of the azimuthal vorticity  $\Omega_\phi$ , the induced azimuthal vorticity  $\omega_\phi$ , attributable to the introduction of the axial vorticity  $\pm|\omega_z|$ , is assumed to be very small, that is,  $|\omega_\phi| < \Omega_\phi$ ; similarly, the induced axial velocity is also assumed to be very small with the assumption that  $|v_z| < U$ . As a result of the

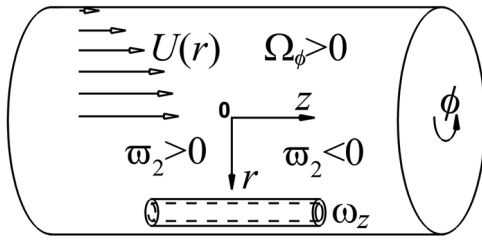


**FIG. 8.** Schematic of the second sign law for the three components of the vorticity distributed within the flow through a circular-section pipe caused by an introduced axial vortex or vortex pair uniformly distributed along the axial direction but periodically varying along the azimuthal direction, where  $U(r)$  (denoted by hollow arrows) is the velocity profile of the pipe flow and  $\Omega_\phi$  is the resultant azimuthal vorticity.

superposition of these two flow fields, for example, in which the f.b.c. with  $k \geq 2$  is employed, we can write the total azimuthal vorticity and axial velocity in  $r \in [R - h, R]$  as follows:

$$\omega_\phi + \Omega_\phi = C_1 z R^{k-1} k [\beta^{-(k+1)} + \beta^{k-1}] \cos(k\phi) + 4\beta R^{-1}, \quad (39)$$

$$v_z + U = C_1 z R^k (\beta^{-k} - \beta^k) \cos(k\phi) + 2(1 - \beta^2). \quad (40)$$

These equations clearly indicate that the appearance of  $\omega_\phi$  is just a quantitative modification of  $\Omega_\phi$  and causes the total azimuthal vorticity and induced axial velocity  $v_z$  with an original velocity  $U(r)$  to sinusoidally vary along the tangential direction. In addition, along the  $\phi$ -axis, the periodically varying total azimuthal vorticity ( $\omega_\phi + \Omega_\phi$ ) and total axial velocity ( $v_z + U$ ) are in phase. Furthermore, the assumption that  $|\omega_\phi| < \Omega_\phi$  corresponds to precondition (A1); otherwise, the invalidation of such an assumption, i.e.,  $|\omega_\phi| > \Omega_\phi$ , could lead to  $|v_z| > U$  and the appearance of the local reversed flow. However, this situation is excluded from the present paper and will be investigated in the future.

Consequently, regarding the evolution of the sign of the vorticity, we have the following modified sign function of the coupled azimuthal vorticity:

$$\text{sgn}(\Omega_\phi + \omega_\phi) = 1, \quad r \in [R - h, R]. \quad (41)$$

With the help of the above analysis and in consideration of the first sign law [Eqs. (35) and (41)], the second sign law for the three components of the vorticity is obtained as follows by introducing the second sign variable,  $\omega_2 = \omega_z \cdot \omega_r \cdot (\Omega_\phi + \omega_\phi)$ , except for some special positions at which  $\omega_2 = 0$  (e.g.,  $\phi = 0$  and  $\lambda$ ),

$$\text{sgn}(\omega_2) = \begin{cases} 1, & z < 0 \\ -1, & z > 0. \end{cases} \quad (42)$$

As shown in Fig. 8, this relationship for the coupled vorticity field shows that the sign of the combination of the three vorticity components is positive upstream and negative downstream relative to the center of the disturbance. Additionally, the wave number  $k$  and Reynolds number  $Re$  are irrelevant to this feature. Interestingly, the second sign law is exactly the same as the sign law in the flow past

the bluff body,<sup>19</sup> i.e., with a negative sign downstream and a positive sign upstream, which further demonstrates that the second sign law is universal in both external and internal flows and is independent of the coordinate system, i.e., the Cartesian system for flat surfaces or a cylindrical system for curved pipe walls.

### C. The third sign law for the radial and axial velocity components

In addition to the two sign laws for the vorticity components above, we obtain the specific relationship, referred to as the third sign law, between the radial and axial components of the induced velocity. By introducing the third sign variable,  $\omega_3 = v_r \cdot v_z$ , and based on Eqs. (2a) and (3) under the specific boundary cases, we have

$$\text{sgn}(\omega_3) = \begin{cases} -1, & z < 0 \\ 1, & z > 0, \end{cases} \quad (43)$$

except for some special positions at which  $\omega_3 = 0$  (e.g.,  $\phi = \frac{1}{2}\lambda$  and  $\frac{3}{2}\lambda$ ). This velocity sign law can also be verified as being consistent with the sign law in the flow past a bluff body,<sup>19</sup> particularly, for a flat plate when  $R \rightarrow \infty$ .

Interestingly, the third sign law is independent of the distribution of the induced tangential velocity  $v_\phi$ , the influence of the original flow  $U(r)$ , the wave number  $k$ , and the Reynolds number  $Re$ ; this also indicates that such a relationship is an intrinsic physical mechanism for the flow through a pipe. Considering that  $\omega_r$  and  $\omega_z$  originate mainly from the 3D disturbed flow field and disappear in the original pipe flow field (except in a turbulent state), the first sign law is easily demonstrated by the iso-surfaces of the vorticity components. However, it is difficult to illustrate the third sign law by the iso-surfaces of the velocity components due to the difficulty in distinguishing the induced velocity components, especially  $v_z$ , from the original pipe flow velocity. With a turbulent flow, in which the induced velocity is regarded as the fluctuating velocity generated by turbulence, some physical phenomena, such as the special sign of the Reynolds stress in a boundary layer on a flat plate, could be better understood or explained.<sup>22</sup>

### D. Examples: Reduced and expanded pipes with a square cross section

Examples to illustrate the above two sign laws for the three vorticity components are briefly presented through direct numerical simulations (DNS). The first kind of secondary flow is adopted by introducing geometric disturbances along the axial and azimuthal directions. As shown in Figs. 9(a) and 10(a), the axial disturbances are represented by the reduction and expansion of the pipe diameter, respectively. The azimuthal disturbance of a square cross section is typically taken into account. Regarding the local disturbed pipe flow, the reduced pipe represents the upstream disturbance because the normal direction of the disturbance points to the inlet, while the expanded pipe represents the downstream disturbance because the disturbance points to the outlet. The reduced and expanded pipes could be compared with conic disturbances upstream and downstream, respectively, as shown in Fig. 1.

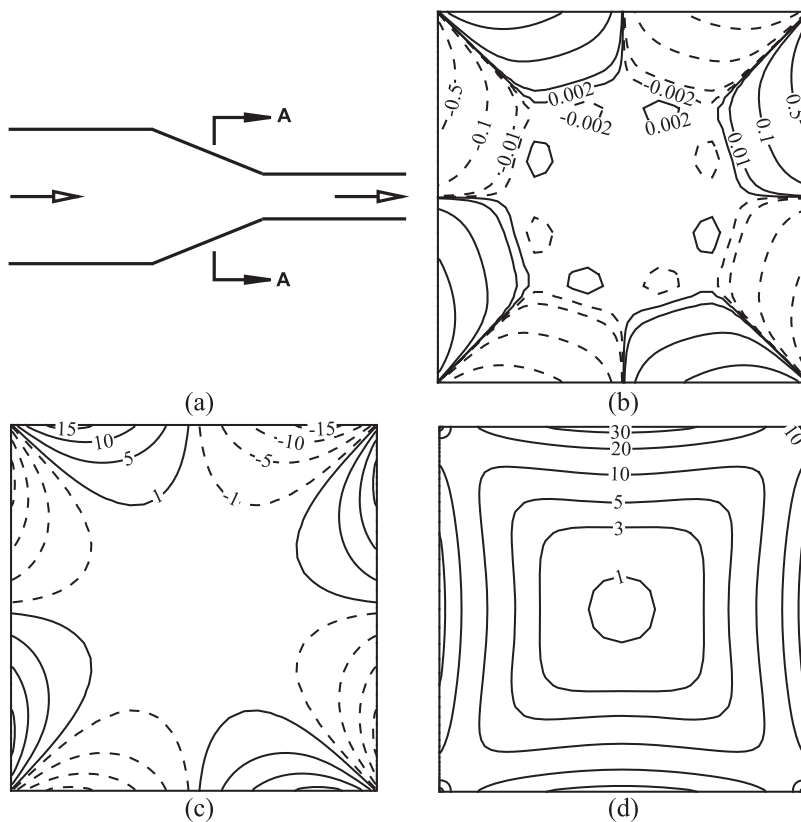


**FIG. 9.** (a) Schematic of the longitudinal section for a reduced pipe and contours of (b)  $\omega_z$ , (c)  $\omega_r$ , and (d)  $\Omega_\phi + \omega_\phi$  in the middle axial position (A-A) with a square cross section at  $Re = 200$ , where solid and dashed lines denote positive and negative values, respectively.

In present DNS, governing equations are written by

$$\nabla \cdot \mathbf{u} = 0, \quad (44a)$$

$$\frac{\partial \mathbf{u}}{\partial t} + (\mathbf{u} \cdot \nabla) \mathbf{u} = -\nabla p + \frac{1}{Re} \nabla^2 \mathbf{u}, \quad (44b)$$

where  $\mathbf{u}$  is the total velocity vector,  $t$  is the time, and  $\nabla$  is the gradient operator. The boundary conditions are presented as follows: (i) the uniform incoming velocity at the inlet; (ii) the simple outflow at the exit; and (iii) non-slip boundary conditions on the walls. In the numerical method, the second-order scheme is applied for both temporal and spatial derivatives, and the SIMPLEC algorithm is adopted in the pressure-velocity coupling.

The spatial distributions of the three vorticity components at the middle axial position of the pipe are presented in Figs. 9 and 10 at  $Re = 200$ , when the flow is laminar and steady without any turbulent disturbance. For the upstream disturbance in Fig. 9, the sign of  $\omega_z$  is always the same as that of  $\omega_r$  in most regions. However, for the downstream disturbance in Fig. 10, the sign of  $\omega_z$  is just opposite to that of  $\omega_r$ , mainly in corners and the central area. Regardless of whether the pipe is reduced or expanded, the sign of  $(\Omega_\phi + \omega_\phi)$  is predominantly positive. Consequently, the first sign law for  $\omega_z \cdot \omega_r$  is strictly valid near the corner region with a strong geometric disturbance. Furthermore, except for the local recirculation in the corners of the expanded pipe, the second sign law always prevails in most regions.

### E. Physical meaning of two vorticity sign laws

As discussed in the previous subsections, for the two vorticity sign laws, there are some similarities in both external flow (EF) past a bluff body and internal flow (IF) through a pipe. The physical meaning can be summarized as follows:

- (i) The first sign law indicates the distorted or inclined direction of the spanwise vortex in EF or the azimuthal vortex in IF, which is already formed in the 2D flow, in the longitudinal section, i.e., the  $x - y$  plane in EF or the  $z - r$  plane in IF;
- (ii) The second sign law illustrates the rotational direction of the 3D vortex predominantly distributed in both EF and IF;
- (iii) Both sign laws indicate that the swirling direction of the 3D primary vortex is specific, rather than random;
- (iv) From the point of the vorticity sign, the special feature in the vorticity vector is newly explained, i.e., there are only two independent components in three vorticity components. Among them, the first sign law clearly indicates the closely dependent relationship between  $\omega_x$  and  $\omega_y$  in EF, as shown in Fig. 1, or between  $\omega_z$  and  $\omega_r$  in IF, as shown in Fig. 9; However, the second sign law just indicates the intrinsic physical relationship between the independent spanwise (EF) or azimuthal (IF) vorticity and the other two vorticity components based on the first sign law.

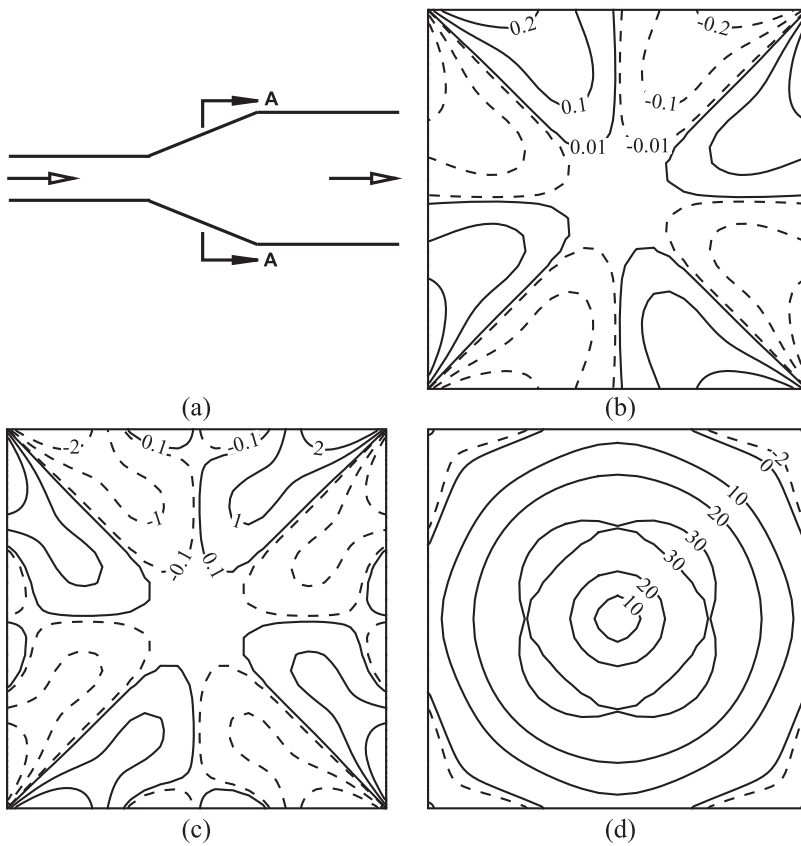


**FIG. 10.** (a) Schematic of the longitudinal section for an expanded pipe and contours of (b)  $\omega_z$ , (c)  $\omega_r$ , and (d)  $\Omega_\phi + \omega_\phi$  in the middle axial position (A–A) with a square cross section at  $Re = 200$ , where solid and dashed lines denote positive and negative values, respectively.

Presently, based on Eq. (44b), the total vorticity transport equation is obtained as follows:

$$\frac{\partial \boldsymbol{\omega}}{\partial t} + (\mathbf{u} \cdot \nabla) \boldsymbol{\omega} = (\boldsymbol{\omega} \cdot \nabla) \mathbf{u} + \frac{1}{Re} \nabla^2 \boldsymbol{\omega}, \quad (45)$$

where  $\boldsymbol{\omega}$  is the total vorticity vector defined as  $\nabla \times \mathbf{u}$ . Therefore, in the immediate neighborhood of walls, Eq. (45) is simplified as

$$\nabla^2 \boldsymbol{\omega} \approx 0. \quad (46)$$

In addition, far away from the walls, there is

$$\frac{\partial \boldsymbol{\omega}}{\partial t} + (\mathbf{u} \cdot \nabla) \boldsymbol{\omega} - (\boldsymbol{\omega} \cdot \nabla) \mathbf{u} \approx 0. \quad (47)$$

Accordingly, as described in the previous assumption (A8), once the vorticity is generated on the walls, the feature of the vorticity sign is determined by Eq. (46). When the vorticity is transported and diffused into the region far away from the walls, the vorticity with a specific sign is invariant due to Kelvin’s circulation theorem in Eq. (47). Therefore, before such vorticity is totally dissipated owing to fluid viscosity, the sign of vorticity is always constant in the present vortex dynamics.

As pointed out in a recent study<sup>23</sup> for EF and discussed in the first sign law, the effect of nonlinear inertial forces including the convection term  $(\mathbf{u} \cdot \nabla) \boldsymbol{\omega}$  and the twisting and stretching terms  $(\boldsymbol{\omega} \cdot \nabla) \mathbf{u}$  can be summarized. As for the first category, i.e., an intermittent or

random disturbance, the only downstream region is valid. While for the second category, i.e., a persistent disturbance, as illustrated in Figs. 9 and 10, the upstream or downstream region is dependent on the introduction of such disturbance, related to the main flow or local flow direction. Therefore, the upstream region for two sign laws only exists in the upstream persistent disturbance, while the downstream region always exists in both types of disturbance.

#### IV. CONCLUSIONS

Based on the VIVor theory in the flow past a bluff body reported in a previous study,<sup>19</sup> the flow through a pipe is investigated as another basic kind of fluid flow, namely, an internal flow. As the first part of the present subject, the features of the vorticity sign are theoretically presented, particularly when secondary flows appear. In the immediate vicinity of the pipe walls where inertial forces can be neglected and viscous forces are dominant, the flow field induced by the introduction of a disturbed vortex or vortex pair as a result of secondary flow is analyzed. Then, two kinds of boundary cases are taken into account: introduced vorticity distributed on the walls and introduced vorticity distributed near the walls (but is absent on the walls).

Considering the typical features of pipe flow, such as taking the form of a paraboloid of revolution, the first sign law for only the radial and axial vorticity components and the second sign law for

the three vorticity components are obtained. Under specific distributions of pipe flow and a resultant azimuthal vorticity that always has a positive sign throughout the pipe, the second sign law is exactly equivalent to the first sign law, i.e., a positive sign upstream and a negative sign downstream. Due to their independence of the induced azimuthal vorticity, original pipe flow, wave number  $k$  of the disturbance, and Reynolds number  $Re$ , these two sign laws are intrinsic physical mechanisms of the evolution of vortices and vorticity dynamics. These laws reveal physical relationships not only among the three vorticity components, but also between the wavy varying total azimuthal vorticity and azimuthal vorticity induced by a 3D perturbation or secondary flow. Furthermore, these sign laws are well consistent with those found in the wake flow of a bluff body if the pipe radius reaches infinity. Finally, examples are briefly illustrated by direct numerical simulations.

The physical meaning of these two vorticity sign laws mainly shows that the rotational direction of the 3D primary vortex in the longitudinal plane is specific. In addition, from the point of the vorticity sign, these sign laws present that two vorticity components in the longitudinal plane are closely dependent, while the original 2D primary vortex normal to the longitudinal plane is independent. Considering the effect of nonlinear inertial forces, the downstream region in both vorticity sign laws only exists for an intermittent or random disturbance, while both the upstream and downstream regions could coexist in a persistent disturbance related to the main or local flow.

In addition, two basic effects of viscous forces are revealed with regard to the physical mechanisms responsible for generating vorticity. The first is the direct effect of viscous forces resulting in two wall-tangent components of vorticity generated on surfaces due to shear flows, such as the introduced vorticity  $\omega_z$  in the present secondary flows. The second is the indirect effect leading to a single wall-normal vorticity component induced by a vortex with former vorticity near the walls, e.g., the vorticity  $\omega_r$  induced by  $\omega_z$  in the present pipe flow. Furthermore, if the (pipe) wall is removed, Kelvin's circulation theory indicates that a 2D introduced vortex or vortex pair is invariable without viscous forces, even under a certain 3D transient disturbance. Even if the fluid is viscous, the main viscous effects, diffusion, and dissipation, would also eliminate such disturbances. Therefore, the wall is necessary for the present indirect effect of viscous forces, indicating that the mechanism of the VIV or is actually a kind of interaction between a vortex and structure.

In the future, as the second part of the present subject, direct numerical simulations of flows through a square-section pipe at the lower Reynolds number will be carried out to verify the characteristics of the first and second sign laws and the relationships with the geometric disturbances that induce secondary flows in non-circular cross sections.

## ACKNOWLEDGMENTS

This work was financially supported by the Strategic Priority Research Program of the Chinese Academy of Science (Grant No. XDB22030101).

## REFERENCES

- H. Schlichting, *Boundary Layer Theory*, 7th ed. (McGraw-Hall Book Company, 1979).
- Y. J. Dai and C. X. Xu, "Wall pressure and secondary-flow origination in a square duct," *Phys. Fluids* **31**, 085104 (2019).
- O. Marin, R. Vinuesa, and P. Schlatter, "Characterization of the secondary flow in hexagonal ducts," *Phys. Fluids* **28**, 125101 (2016).
- A. Vidal, R. Vinuesa, P. Schlatter, and H. M. Nagib, "Influence of corner geometry on the secondary flow in turbulent square ducts," *Int. J. Heat Fluid Flow* **67**, 69–78 (2017).
- A. Vidal, H. M. Nagib, P. Schlatter, and R. Vinuesa, "Secondary flow in spanwise-periodic in-phase sinusoidal channels," *J. Fluid Mech.* **851**, 288–316 (2018).
- M. De Marchis, B. Milici, and E. Napoli, "Numerical observations of turbulence structure modification in channel flow over 2D and 3D rough walls," *Int. J. Heat Fluid Flow* **56**, 108–123 (2015).
- P. Orlandi and S. Leonardi, "DNS of turbulent channel flows with two- and three-dimensional roughness," *J. Turbul.* **7**, N73 (2006).
- X. I. A. Yang, J. Sadique, R. Mittal, and C. Meneveau, "Exponential roughness layer and analytical model for turbulent boundary layer flow over rectangular-prism roughness elements," *J. Fluid Mech.* **789**, 127–165 (2016).
- M. J. P. Kevin, H. L. Bai *et al.*, "Cross-stream stereoscopic particle image velocimetry of a modified turbulent boundary layer over directional surface pattern," *J. Fluid Mech.* **813**, 412–435 (2017).
- J. Yang and W. Anderson, "Numerical study of turbulent channel flow over surfaces with variable spanwise heterogeneities: Topographically-driven secondary flows affect outer-layer similarity of turbulent length scales," *Flow, Turbul. Combust.* **100**, 1–17 (2018).
- L. Chan, M. MacDonald, D. Chung, N. Hutchins, and A. Ooi, "Secondary motion in turbulent pipe flow with three-dimensional roughness," *J. Fluid Mech.* **854**, 5–33 (2018).
- H. F. Liu, "An investigation on oil-water separation in cylindrical cyclone," Ph.D. dissertation (Institute of Mechanics, Chinese Academy of Sciences, 2012) (in Chinese).
- J. Carlos Berrio, E. Pereyra, and N. Ratkovich, "Computational fluid dynamics modelling of gas-liquid cylindrical cyclones, geometrical analysis," *J. Energy Resour. Technol.* **140**, 092003 (2018).
- S. Y. Shi and J. Y. Xu, "Flow field of continuous phase in a vane-type pipe oil-water separator," *Exp. Therm. Fluid Sci.* **60**, 208–212 (2015).
- F. Yang, A. Liu, and X. Guo, "Numerical simulation on the performance of axial vane type gas-liquid separator with different guide vane structure," *Int. J. Fluid Mach. Syst.* **10**, 86–98 (2017).
- F. Zhou, G. Sun, X. Han, Y. Zhang, and W. Bi, "Experimental and CFD study on effects of spiral guide vanes on cyclone performance," *Adv. Powder Technol.* **29**, 3394 (2018).
- L. M. Lin, X. F. Zhong, and Y. X. Wu, "Effect of perforation on flow past a conic cylinder at  $Re = 100$ : Vortex-shedding pattern and force history," *Acta Mech. Sin.* **34**, 238–256 (2018).
- L. M. Lin, X. F. Zhong, and Y. X. Wu, "Effect of perforation on flow past a conic cylinder at  $Re = 100$ : Wavy vortex and sign laws," *Acta Mech. Sin.* **34**, 812–829 (2018).
- L. M. Lin, S. Y. Shi, X. F. Zhong, and Y. X. Wu, "Mechanism of wavy vortex and sign laws in flow past a bluff body: Vortex-induced vortex," *Acta Mech. Sin.* **35**, 1–14 (2019).
- P. K. Kundu, I. M. Cohen, and D. R. Dowling, *Fluid Mechanics*, 5th ed. (Academic Press, 2012), ISBN: 978-0-12-382100-3.
- S. I. Green, *Fluid Vortices* (Kluwer Academic Publishers, Norwell, 1995).
- L. M. Lin and Y. X. Wu, "New interpretation of specific sign of Reynolds stress in the boundary layer on a flat plate," *Theor. Appl. Mech. Lett.* **8**, 372–377 (2018).
- L. M. Lin, "Vorticity sign law in three-dimensional wake of bluff body at low Reynolds number," *Acta Phys. Sin.* **69**, 034701 (2020) (in Chinese).